Arabian Journal of Chemistry (2023) **16**, 104965

King Saud University

Arabian Journal of Chemistry

www.ksu.edu.sa
www.sciencedirect.com

ORIGINAL ARTICLE

MHD mixed convection flow for Maxwell Hybrid nanofluid with Soret, Dufour and Morphology effects

Abdul Rauf [a,1], Fiaz Hussain [a], Aqsa Mushtaq [a], Nehad Ali Shah [b,1], Mohamed R. Ali [c,d,*]

[a] *Department of Mathematics, Air University Multan Campus, Chak 5-Faiz, Bahawalpur Road, Multan, Pakistan*
[b] *Department of Mechanical Engineering, Sejong University, Seoul 05006, South Korea*
[c] *Faculty of Engineering and Technology, Future University in Egypt, New Cairo 11835, Egypt*
[d] *Basic Engineering Science Department, Benha Faculty of Engineering, Benha University, Benha, Egypt*

Received 11 February 2023; accepted 26 April 2023
Available online 4 May 2023

KEYWORDS

Nano-fluid;
Maxwell hybrid nano-fluid;
Soret and Dufour effects;
Mixed convection flow;
Nanoparticle Shape Factor

Abstract We have investigated the two-dimensional mixed convective Maxwell hybrid nanofluid boundary layer mass and heat flows over a linearly stretching porous surface with the applied external magnetic flux. Thermal radiations along with the Dufour and Soret effects are also incorporated. The governing model of partial differential equations (PDE) is altered into ordinary differential equations (ODE) with an appropriate similarity transformation. The finite difference-based numerical method BVP4c is applied to solve the system of nonlinear ODEs. The flow features and the heat transfer characteristics have been illustrated with graphical representations and a numerical table. For varied values of the flow-related variables, organized and graphical data for the Nusselt number and skin friction coefficient are indicated. In most cases, spherical-shaped nanoparticles have a better influence on stream function, velocity and temperature distributions. This behavior is the opposite of the mass concentration profile. It has been observed that stream function decreases as increase the value of the magnetic field but opposite for mass concentration distribution and temperature profile. The temperature gradient is enhanced as a result of stronger convective flow when Soret number Sr values increase, which causes the boundary layer thickness to grow. A comparative study of hybrid nanofluid and nanofluid showed that the hybrid nanofluid has superior shear stress/skin friction and Sherwood number/surface mass flux than nanofluid flow.

* Corresponding author.
E-mail addresses: attari_ab092@yahoo.com (A. Rauf), muhammadshahid42791@gmail.com (F. Hussain), aqsamushtaq22@gmail.com (A. Mushtaq), nehadali199@sejong.ac.kr, nehadali199@yahoo.com (N. Ali Shah), mohamed.reda@fue.edu.eg (M.R. Ali).

[1] These authors contributed equally to this work and are co-first authors.

https://doi.org/10.1016/j.arabjc.2023.104965
1878-5352

Nomenclature

β	Maxwell fluid parameter	a	amplitude of wave surface
λ	time period of thermal relaxation	T_m	temperature of mean fluid
β_T	temperature volume expansion's coefficient	λ_1	mixed convection parameter
k_T	thermal diffusion ratio	λ_3	concentration buoyancy parameter
λ_2	thermal buoyancy parameter	U_w	uniform wall velocity
N_t	thermophoretic parameter	C	concentration
T	temperature	k_{s1}	firsts nanoparticle thermal conductivity
T_w	*wall temperature*	k_f	base fluids thermal conductivity
k_{s2}	second nanoparticle thermals conductivity	k_{hnf}	hybrid nanofluids thermals conductivity
k_{nf}	thermals conductivity of the nanofluid	ρ_{s2}	second nanoparticle density
ρ_{s1}	first nanoparticle density	D	diffusivity of fluid
$(c_p)_{hnf}$	Specifics heats of the hybrid nanofluid	M	magnetic field parameter
k	the porosity parameter	S_r	Soret number
μ	viscosity of the fluid	μ_{hnf}	hybrid nanofluid's dynamic viscosity
Pr	Prandtl number	D_f	Dufour number
ρ_{hnf}	hybrid nanofluid density	Le	Lewis number
σ_{hnf}	hybrid nanofluid's thermal conductivity	C_f	skin friction coefficient
υ_{hnf}	hybrid nanofluid's kinematic viscosity	R_{ex}	local Reynolds number
c_p	Specifics heat of the fluid	q_m	mass flux
g	Gravitational acceleration ms^{-2}	η	variable of similarity
U_∞	uniform free stream velocity	γ	dimensionless porosity parameter
θ	Temperature distribution without dimensions	υ	kinematic viscosity
μ	dynamic viscosity	δ	fluid's thermal porosity
ρ	density	∞	ambient condition
σ	electric conductivity of the fluid	Φ_2	second volume fraction of nanoparticle
Φ_1	first volume fraction of nanoparticle		
β_c	concentration volume expansion's coefficient		

1. Introduction

Researchers are studying mathematical simulations for non-Newtonian fluids because of the expanding tendency in technological and industrial applications. Non-Newtonian fluids are used in a variety of applications, including extrusion of metal, metal whirling, lubricant industrial for a wide range of vehicles, the molten metal distillation from non-metallic insertion, shoe business (the shoe must be filled with an exact non-Newtonian fluid to defend feet from wounds), the pharmaceutical and food sectors, and as a means of cooling. Various academics have provided non-Newtonian fluids with mathematical models to analyze their properties over time. One prominent category of mathematical models is the Maxwell model. The non-Newtonian Maxwell fluid model may forecast the temporal relaxation phenomenon, which is not achievable with the Newtonian model. Various scholars have used this model in different flow scenarios.(See Fig. 1)

The manufacturing industry relies heavily on flow and heat transmission from thermal radiation for the construction of reliable machinery, gas turbines, nuclear power plants, weapons, satellites, and spacecraft. Because heat transmission and radiative flux are significantly more important at high temperatures. The energy balance for the first and second Rayleigh–Stokes problems of the Maxwell fluid was studied by Zierep and Fetecau (Zierep and Fetecau, 2007) under the influence of varied initial and boundary circumstances. Fetecau et al. (Fetecau et al., 2009) also demonstrated an unstable flow of fractional derivatives in the Maxwell fluid under the outcome of a constant-speed accelerating plate. Choi (Choi, 1995) coined the word nanofluids, which refers to suspended nanoparticles, and it has changed the modern period owing to its varied range of engineering and technological applications. When a modest number of nanoparticles (usually comprised of Ag, Au, Al, or their oxides) sized from 1 to 100 nm is added into normal base fluids, nanofluids stimulate thermal conductivity and heat transfer rate (water, glycol, ethylene, oil). Nanofluids are the subject of several investigations. Shehzad et al. (Shehzad et al., 2016) looked studied three-dimensional Nanofluid flow by Jeffrey with internal heat production and thermal radiation. The entire inquiry is carried out with convective boundary circumstances in mind. Sisko nanofluid three-dimensional flow with an MHD boundary layer was investigated by Hayat et al. (Hayat, xxxx). Stretching the surface in two directions generates the flow. Khan et al. (Technol, 2016) studied the 3-D flow of a spinning nanofluid that encouraged a flexible surface heated convectively. They discussed nanofluid flow under the impact of thermal conductivity using two different models. Dogonchi and Ganji (Dogonchi and Ganji, 2016) used the Duan–Rach methodology, which is an improved variant of the Adomian Decomposition method, MHD radiative viscous nanofluid flow amid stretching/shrinking barriers was investigated. A chemical reaction solution for MHD three-dimensional visco-elastic nanofluid flow was provided by Ramzan and Bilal (Ramzan and Bilal, 2016). They employed HAM to determine the problem's series solution. Refs. (Kumar et al., 2022; Sajjan et al., 2022; Abderrahmane

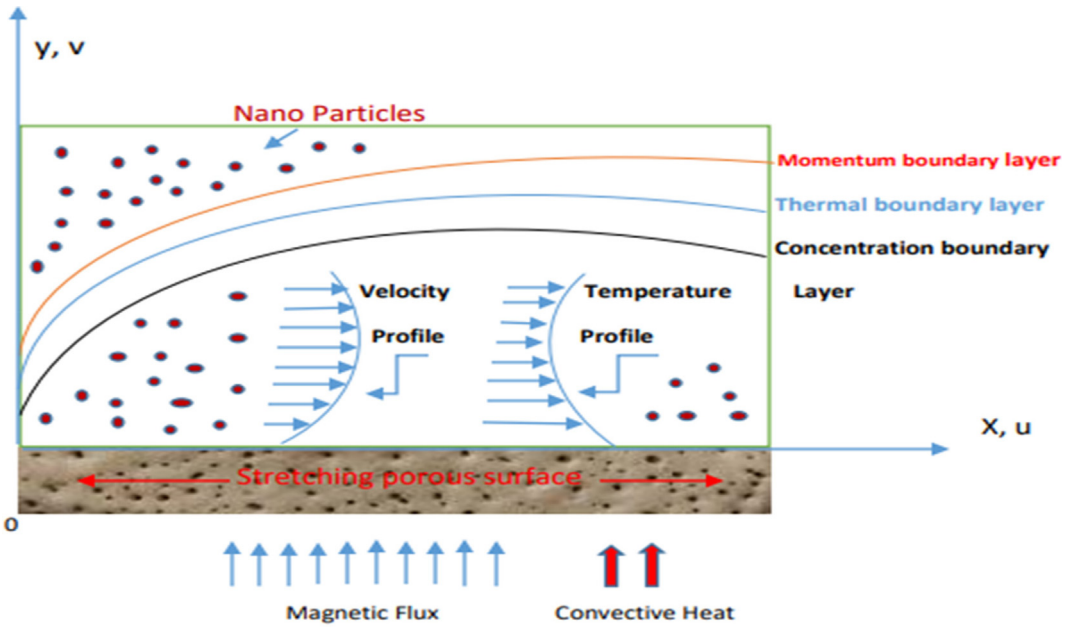

Fig. 1 The geometry of the flow

et al., 2022; Rauf et al., 2022) provide further information on the study of the hybrid nanoparticle effect.

To study heat-related energy transfer involving nano liquids, Buongiorno (Buongiorno, 2006) developed a two-phase model. Using the Buongiorno model, Akbar et al. (Akbar, xxxx) investigated natural convection influences on MHD double-diffusive nanofluid flow and discovered dual solutions for the stretching parameter. Since of its diverse geophysical and technical uses, such as some essential oils, low shear rates of blood, dyes, cleanse, polymers, fluids with colloidal particles, goods for cosmetics, pasta, liquids in suspension, ice cream, flour for making dough, sludge, and so on, the study of non-Newtonian fluids has been a hot subject among scientists and researchers in recent years. In drilling operations, the food business, and biotechnology, these fluids can be natural or manufactured, and they include oils, water, red cells, unit, and stretched chain particles.

The effects of activation energy and chemical reaction with buoyant influences on MHD nano liquid flow past a vertical surface were investigated by Mustafa et al. (Mustafa et al., 2017). Using a parameter control technique, Hsiao (Hsiao, 2017) examined the effects of activation energy thermal extrusion industrialized structure output on the development of radiation electrical magneto-Carreau nano liquid flow. In the presence of chemical reactivity, Zeshan et al. (Zeeshan et al., 2018) addressed the significance of activation energy in Couette-Poiseuille nanofluid flow. Hassan et al. (Hassan et al., 2018) investigate the convective heat transmission in nanofluid flow in a porous medium over a wavy surface. Additional details on the investigation of Maxwell fluid movement involving activation energy can be found in references (Ahmad and Khan, 2019; Layek et al., 2018; Khan et al., 2020; Ahmad and Khan, 2019; Mukhopadhyay et al., 2005).

The resulting fluids interact in a nonlinear way between dynamic viscosity and shear rate. The structures of non-Newtonian fluids cannot be revealed by a single constitutive equation. That is why researchers utilize a range of non-Newtonian fluid models in their research, both theoretical and practical (Shafique et al., 2016; Khader and Megahed, 2016; Abbas et al., 2016; Ramzan et al., 2013; Türk and Sezgin, 2016; Ramzan et al., 2015; Hayat et al., 2016; Hayat et al., 2014; Ramzan et al., 2016). The relevance of boundary layer non-Newtonian flows was highlighted by applications in the industry such as photographic films with a liquid coating, meal preparation, the condensing of a film, and reclaiming oil. The flow of stretched boundary layer is especially important in terms of technical and industrial applications including extrusion of metal, paper manufacture, glass fibre, hot rolling, film made from plastic, and illustration of a wire. Mustafa et al. (Mustafa et al., 2016) looked at a 3D rotating ferrofluid flow created by a radiative surface under magnetohydrodynamic influences. With a new notion of radiative heat flow in nonlinear form, a combination of nanoparticles Fe_3O_4 is suggested. Ali et al. (Ali et al., 2016) examined the impact of Dufour and MHD Soret on viscoelastic flow in the second grade via a stretched sheet that oscillates and is permeable with heat radiation.

The Homotopy analysis method is used to resolve this issue. MHD Casson nanofluid flow across a nonlinear vertical

Table 1 Thermophysical characteristics of nanofluid and the base fluid (Rauf et al., 2023).

Properties	base fluid	Nano-particle	
	Ethylene glycol (EG)	AL_2O_3	Cu
$C_P(j/KgK)$	2415.5	765.0	385.0
$\rho(kg/m^3)$	1114.0	3970.0	8933
$K(W/mK)$	0.2520	40.0	400.0
$\sigma(s/m)$	5.50×10^{-6}	59.6×10^{6}	35×10^{6}
$\beta^* \times 10^{-5}K^{-1}$	6.50	0.850	1.670

stretching surface under the influence of heat radiation and ohmic dissolution was investigated by Pal et al. (Pal et al., 2016). Scaling group transformations are applied to convert boundary layer partial differential equations (PDE) to ordinary differential equations (ODE). The problem is solved using RKF 5th order methodology and the shooting method. Mabood and Pochai (Mabood and Pochai, 2016) investigated the solution of MHD viscous fluid flow through a nonlinear porous extended sheet using optimal Homotopy analysis. The boundary layer flow of the Maxwell fluid was addressed by Renardy and Wang ([37]). Hayat et al. (Hayat et al., 2011) observed the impact of mass transfer on Maxwell liquid inaction point flow. In a 2D stretched surface for Maxwell flow, Hayat et al. (Hayat et al., 2011) investigated the impact of mass transmission on a time-dependent MHD flow. Falkner–Skan flow with MHD Maxwell fluid, Abbas bandy (Abbasbandy et al., 2014) performed analytical and numerical solutions. Mustafa et al. (Mustafa et al., 2015) looked at stable flow in viscoelastic Maxwell nanofluids. Awais et al. (Awais et al., 2015) investigate Maxwell nanofluid boundary layer flow with heat production and absorption. Ramzan et al. utilised the BVPh. 2.0 Mathematica Package to investigate the Dufour and Soret effects of Maxwell nanofluid for a mixed convection flow through extending vertical porous surface to the outside. Refs. (Sidra et al., 2017; Asim et al., 2018; Alireza et al., 2018) provide further information on the study of Maxwell fluid flow.

A thorough review of the literature reveals that no studies on the analysis of heat and mass transfer for mixed convection, thermal radiation, with Soret, Dufour, and Morphology effects of Maxwell hybrid nanofluid flow over a linearly stretching porous surface with an applied external magnetic flux have been conducted. In this paper, we consider this flow. The linear stretching surfaces have a proportionate connection between temperature, velocity, and concentration boundary layer, according to an examination of major literature on mixed convection flow

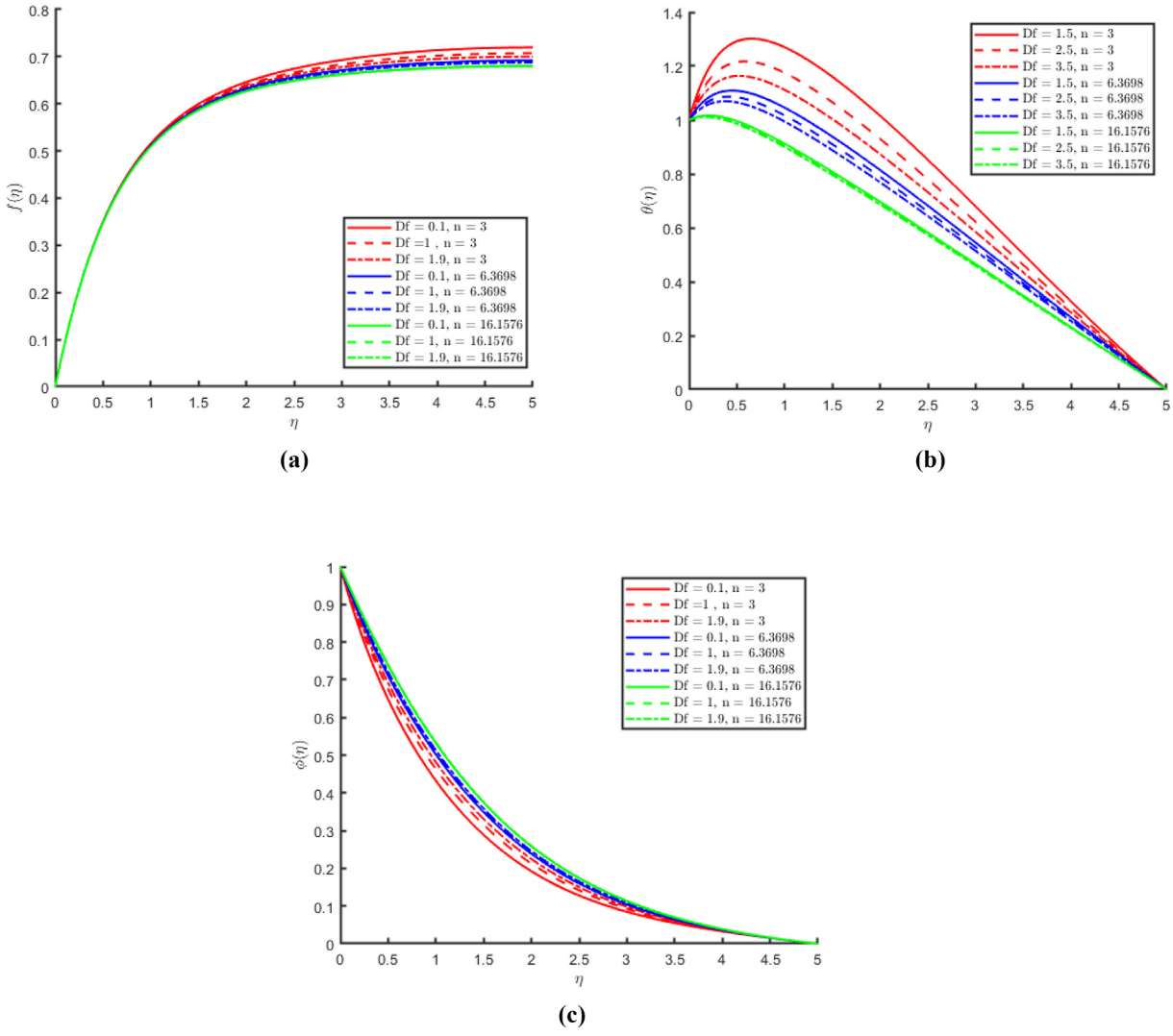

Fig. 2 (a) Representation of the effect of Dufour on the stream function $f(\eta)$ with different nanoparticle shape sizes. (b) Representation of the effect of Dufour on the temperature $\theta(\eta)$ with different nanoparticle shape sizes. (c) Representation of the effect of Dufour on the mass concentration $\phi(\eta)$ with different nanoparticle shape sizes

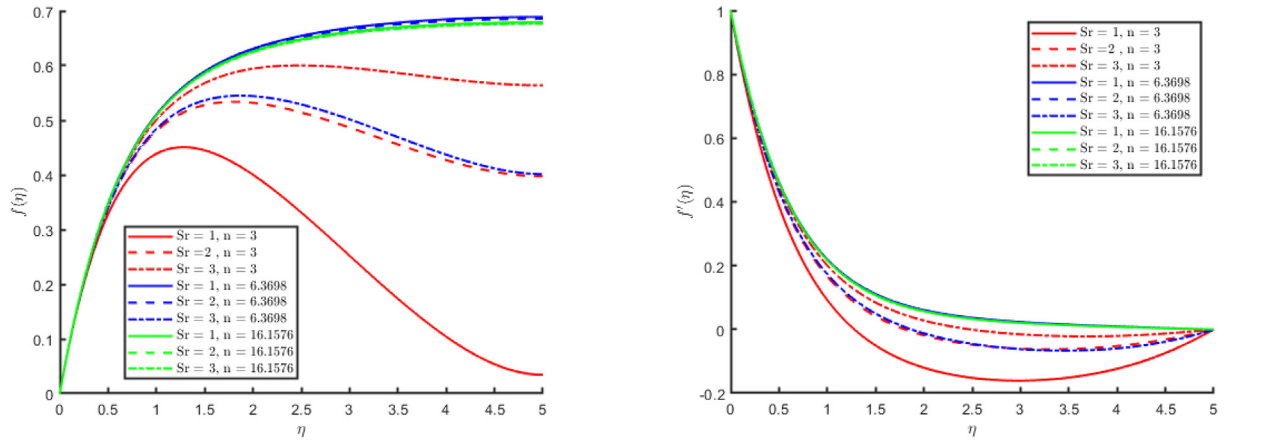

(a) **(b)**

Fig. 3 (a) Representation of the effect of Soret number on the stream function $f(\eta)$ with different nanoparticle shape sizes. (b) Representation of the effect of Soret on the velocity $f'(\eta)$ with different nanoparticle shape sizes

2. Generic Model of Maxwell fluid

Macromolecular or polymeric fluids include Maxwell fluids. Numerous tests suggest that polymeric fluids have both elastic and viscous characteristics (Bird et al., 1987). They differ significantly from tiny molecular fluids as a result. The latter are properly described by Newton's law of viscosity and have viscosity as their primary characteristic.

$$\tau = -v\,[\nabla v + (\nabla v)^T - \tfrac{2}{3}\nabla \cdot vI] - \kappa\nabla \cdot vI, \text{ (a)}$$

and also known as Newtonian fluids. Here $\tau = \tau(x,t)$ is the stress tensor of the fluid at space-time (x,t), v is the shear viscosity, κ is the bulk viscosity, $v = v(x,t)$ is the velocity, ∇ is the gradient operator concerning the space variable $x = (x_1, x_2, x_3)$, the superscript T stands for the transpose operator and I denotes the unit matrix of order 3. The traditional Navier- Stokes equations are obtained by combining Newton's law of viscosity with the conservation rules of mass, momentum, and energy. Maxwell developed the following constitutive relation to explain the elastic characteristics of polymeric fluids by combining Hooke's law of elasticity and Newton's law of viscosity (Maxwell and "iv., 1867).

$$\varepsilon\tau_t + \tau = -v[\nabla v + (\nabla v)^T - \tfrac{2}{3}\nabla \cdot vI] - \kappa\nabla \cdot vI. \text{ (b)}$$

The ratio of viscosity to elastic modulus is shown here ε. The constitutive connection is seen in a Maxwell fluid (b). This relationship illustrates how the stress tensor reacts to fluid motion in a delayed rather than instantaneous manner. Numerous additional nonlinear and realistic constitutive relations, such as the well-known upper-convected Maxwell (UCM) and Oldroyd-B models, were inspired by it (Deville and Gatski, 2012).

27736807994910400**Mathematical formulation**

Consider a 2-dimensional non–Newtonian, incompressible laminar flow electrically conducted boundary layer mixed convective radiative Maxwell hybrid nanofluid flow with velocity $u = ax$ over a linearly stretched surface in the existence of Dufour, Soret effects, and applied thermal conductivity. In the regular path-to-flow system, a strong external magnetic field B_0 is applied. Thermal radiation is unified into the temperature equation and simplified using assumption. The system of governing equations is as follows (Jawad et al., 2021):

$$\frac{\partial u}{\partial x} + \frac{\partial v}{\partial y} = 0, \tag{1}$$

$$v\frac{\partial u}{\partial y} + u\frac{\partial u}{\partial x} + \beta\left(v^2\frac{\partial^2 u}{\partial y^2} + u^2\frac{\partial^2 u}{\partial x^2} + 2uv\frac{\partial^2 u}{\partial x \partial y}\right) = \upsilon_{hnf}\frac{\partial^2 u}{\partial y^2} - \frac{\delta_{hnf}B_0^2}{\rho_{hnf}}u + g\frac{(\rho\beta_T)_{hnf}}{\rho_{hnf}}(T - T_\infty) + g\frac{(\rho\beta_c)_{hnf}}{\rho_{hnf}}(C - C_\infty) - \frac{\upsilon_{hnf}}{K}u \tag{2}$$

$$u\frac{\partial T}{\partial x} + v\frac{\partial T}{\partial y} = \frac{k_{hnf}}{(\rho cp)_{hnf}}\frac{\partial^2 T}{\partial y^2} + \frac{1}{\left(\rho c_p\right)_{hnf}}\frac{\partial q_r}{\partial y} + \frac{\mu_{hnf}}{(\rho cp)_{hnf}}\left(\frac{\partial u}{\partial y}\right)^2 + \frac{\sigma_{hnf}}{\left(\rho c_p\right)_{hnf}}B_o^2u^2 + \frac{Q_0}{\left(\rho c_p\right)_{hnf}}(T - T_\infty) + \left[D_b\frac{\partial C}{\partial y}\frac{\partial T}{\partial y} + \frac{D_t}{T_\infty}\left(\frac{\partial T}{\partial y}\right)^2\right] + \frac{D_t k_T}{T_\infty}\frac{\partial^2 T}{\partial y^2} \tag{3}$$

$$u\frac{\partial C}{\partial x} + v\frac{\partial C}{\partial y} = \left(\frac{D_t K_T}{T_\infty}\right)\left(\frac{\partial^2 T}{\partial y^2} + \frac{\partial^2 T}{\partial x^2}\right) + D_b\left(\frac{\partial^2 C}{\partial x^2} + \frac{\partial^2 C}{\partial y^2}\right) \tag{4}$$

where u and v are velocity components in the x-direction and y-direction respectively, Brownian diffusion coefficient is D_B, the thermophoretic diffusion coefficient is D_t, the thermal radiation flux is q_r, the permeability constant K, the density is ρ, kinematic viscosity is v, the specific heat is ρc_p, Deborah number is D_e, concentration susceptibility is C_s, the thermal diffusion coefficient is k_T, C is concentration, T is temperature, p is pressure, the strong magnetic field is M, and the porosity parameter is k respectively.

The Roseland approximation for the radiative heat flux vector q_r is given by

$$q_r = -\frac{4\sigma^*}{3K^*}\frac{\partial T^4}{\partial y} \tag{5}$$

Where K^* and σ^* are respectively the coefficient of mean absorption and Stefan Boltzmann constant. The variance in temperature within the flow is presumed to be adequately tiny such that T^4 can be represented as a linear temperature function that is achieved by expanding over T_∞ in Taylor's series and ignoring the terms of higher-order, thereby

$$T^4 \approx 4T_\infty T - 3T_\infty^4 \tag{6}$$

Then using (5) and (6), equation (3) reduces to

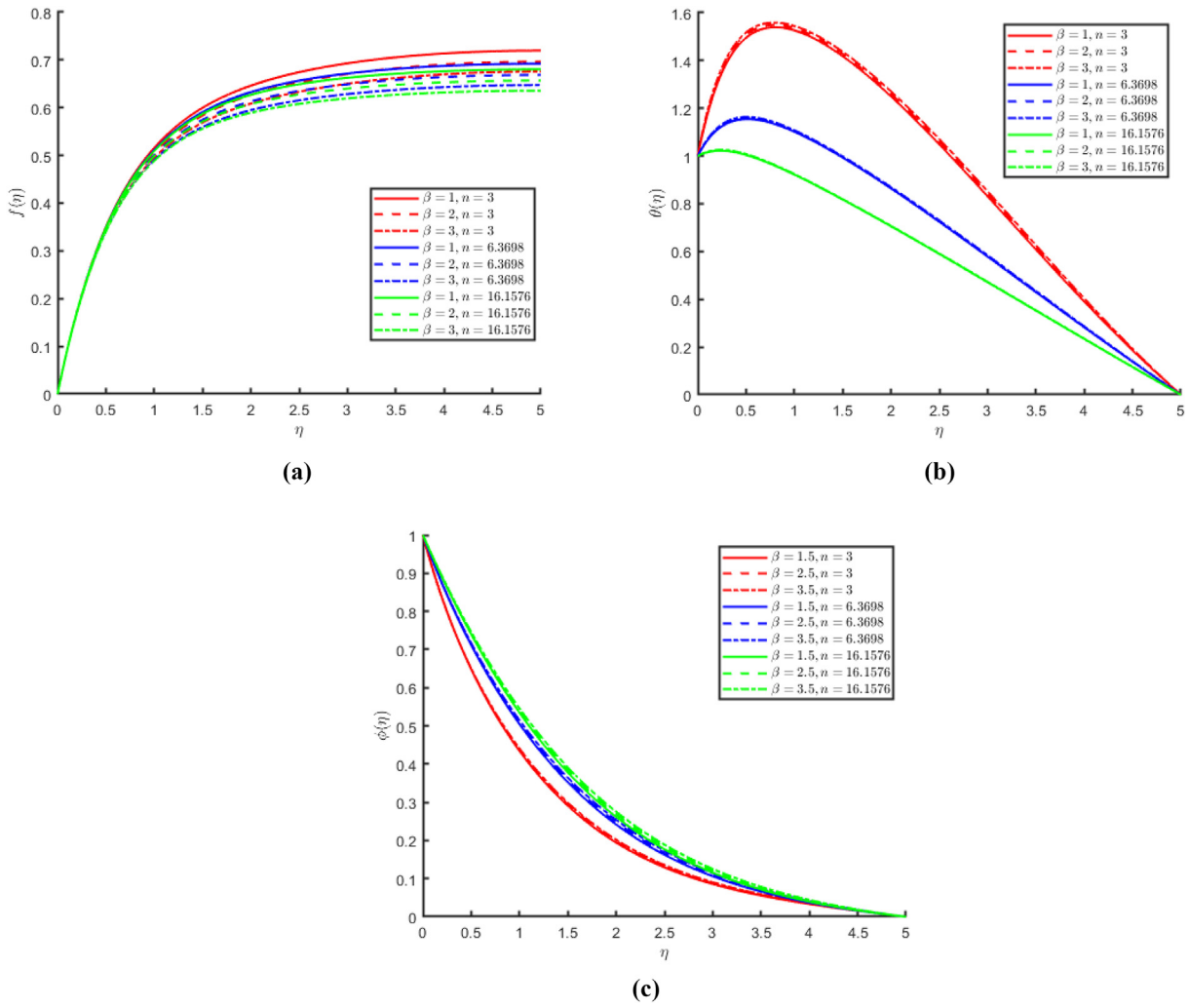

Fig. 4 (a) Representation of the effect of Maxwell parameter on the stream function $f(\eta)$ with different nanoparticle shape sizes. (b) Representation of the effect of Maxwell parameter on the temperature $\theta(\eta)$ with different nanoparticle shape sizes . (c) Representation of the effect of Maxwell parameter on the mass concentration $\phi(\eta)$ with different nanoparticle shape sizes

$$u\frac{\partial T}{\partial x}+v\frac{\partial T}{\partial y}=\left(\frac{k_{hnf}}{(\rho cp)_{hnf}}+\frac{1}{(\rho c_p)_{hnf}}\frac{16\sigma^* T_\infty^*}{3K^*}\right)\frac{\partial^2 T}{\partial y^2}+\frac{\mu_{hnf}}{(\rho cp)_{hnf}}\left(\frac{\partial u}{\partial y}\right)^2+\frac{\sigma_{hnf}}{(\rho c_p)_{hnf}}B_o^2u^2 +\frac{Q_0}{(\rho c_p)_{hnf}}(T-T_\infty)+\left[D_b\frac{\partial C}{\partial y}\frac{\partial T}{\partial y}+\frac{D_t}{T_\infty}\left(\frac{\partial T}{\partial y}\right)^2\right]+\frac{D_tk_T}{T_\infty}\frac{\partial^2 T}{\partial y^2} \tag{7}$$

The values of μ_{hnf}, σ_{hnf}, ρ_{hnf}, $(\rho C_p)_{hnf}$, $(\rho\beta_T)_{hnf}$, $(\rho\beta_c)_{hnf}$ and k_{hnf} for hybrid nanofluid (Al_2O_3-Cu/EG) are defined as (Ishak et al., 2009);

$$\frac{\mu_{hnf}}{\mu_f}=\frac{1}{(1-\Phi_1)^{2.5}(1-\Phi_2)^{2.5}} \tag{8}$$

$$\frac{\sigma_{hnf}}{\sigma_{bf}}=\frac{2\sigma_f+\sigma_{s2}-2\Phi_2(\sigma_{bf}-\sigma_{s2})}{2\sigma_{bf}+\sigma_{s2}+\Phi_2(\sigma_{bf}-\sigma_{s2})}, \tag{9}$$

where

$$\frac{\sigma_{bf}}{\sigma_f}=\frac{2\sigma_f-2\Phi_2(\sigma_f-\sigma_{s2})+\sigma_{s2}}{2\sigma_f+\sigma_{s1}+\Phi_1(\sigma_f-\sigma_{s1})}$$

$$\rho_{hnf}=(1-\Phi_2)[(1-\Phi_1)\rho_f+\Phi_1\rho_{s1}]+\Phi_2\rho_{s2}, \tag{10}$$

$$(\rho c_p)_{hnf}=[\Phi_1(\rho c_p)_{s1}]+\Phi_2(\rho c_p)_{s2}+(1-\Phi_2)[(1-\Phi_1)(\rho c_p)_f]$$

$$(\rho\beta_T)_{hnf}=[\Phi_1(\rho\beta_T)_{s1}]+\Phi_2(\rho\beta_T)_{s2}+(1-\Phi_2)[(1-\Phi_1)(\rho\beta_T)_f]$$

$$(\rho\beta_C)_{hnf}=[\Phi_1(\rho\beta_C)_{s1}]+\Phi_2(\rho\beta_C)_{s2}+(1-\Phi_2)[(1-\Phi_1)(\rho\beta_C)_f] \tag{11}$$

$$\frac{k_{hnf}}{k_{bf}}=\frac{(n-1)k_f+k_{s2}-(n-1)\Phi_2(k_{bf}-k_{s2})}{(n-1)k_{bf}+k_{s2}+\Phi_2(k_{bf}-k_{s2})}, \tag{12}$$

where

$$\frac{\dot{k}_{bf}}{\dot{k}_f}=\frac{(n-1)k_f-(n-1)\Phi_2(k_f-k_{s2})+k_{s2}}{(n-1)k_f+k_{s1}+\Phi_1(k_f-k_{s1})}$$

Φ_1, Φ_2 are the volume fractions of solid nanoparticles such as Aluminum and copper respectively.

The boundary conditions of the problem are

$$u=ax, v=0, C=C_w, T=T_w, aty=0$$

$$u = 0, C \to C_\infty, T \to T_\infty, at\ y \to \infty \tag{13}$$

To solve adequately these nonlinear differential equations, we utilized similarity transformation

$$v = -\sqrt{av}f(\eta), u = axf'(\eta), \eta = \sqrt{\frac{a}{v}}y, \theta(\eta) = \frac{T - T_\infty}{T_w - T_\infty}, \phi(\eta) = \frac{C - C_\infty}{C_w - C_\infty} \tag{13}$$

By using similarity transformation (13), Eq. (1) is satisfied identically, while Eqs. (2), (3) and (7) converted to

$$f'^2 - f''f + a\beta(f''''f^2 - 2f''f'f) = \frac{e_1}{e_2}f''' - \frac{e_3 M}{e_2}f' + \frac{e_4}{e_2}\lambda\theta + \frac{e_5}{e_3}\lambda_1\phi - \frac{e_1}{e_6}\gamma f'$$

$$-f\theta' = (\frac{e_6}{e_7}\chi_1 + Rd)\theta'' + \frac{1}{e_7}\Pr\chi\theta + Nb\phi'\theta' + Nt\theta' + D_f\theta'' + \frac{e_1}{e_7}Ec.\Pr f''^2 + \frac{e_3}{e_7}Ec\Pr M_0 f'^2$$

$$\phi'' = -LeSr\theta'' - Le\phi' f \tag{16}$$

with the boundary conditions

$$f'(\infty) = 0, \theta(\infty) = 0, \phi(\infty) = 0, f'(0) = 0, f(0) = 0, \theta(0) = 1, \phi(0) = 1. \tag{17}$$

and the dimensionless parameters are

$$M = \frac{\sigma_f B_0^2}{\rho_f a}\lambda = \frac{(g\beta_T)_f(T_w - T_\infty)}{a^2}\lambda_1 = \frac{(g\beta_c)_f(c_w - c_\infty)}{a^2\rho_f}$$

$$\gamma = \frac{v_f}{Ka}e_1 = \frac{\mu_{hnf}}{\mu_f}e_3 = \frac{\sigma_{hnf}}{\sigma_f}e_2 = \frac{\rho_{hnf}}{\rho_f}e_4 = \frac{(\rho\beta_T)_{hnf}}{(\rho\beta_T)_f}$$

$$e_5 = \frac{(\rho\beta c)_{hnf}}{(\rho\beta c)_f}e_6 = \frac{k_{hnf}}{k_f}D_f = \frac{D_t k_T}{vT_\infty}$$

$$S_r = \frac{D_t k_T(T_w - T_\infty)}{T_\infty v(C_w - C_\infty)}N_t = \frac{D_t(T_w - T_\infty)}{T_\infty v}L_e = \frac{v}{D_b}$$

$$N_b = \frac{D_b(C_W - C_\infty)}{v}\Pr = \frac{(\rho c_p)_f}{k_f}e_7 = \frac{(\rho c_p)_{hnf}}{(\rho c_p)_f}$$

$$Rd = \frac{16\sigma^* T_\infty^*}{3K^* v(\rho c_p)_f}Ec = \frac{a^2x^2}{v(\rho c_p)_f(T_w - T_\infty)}M_0 = \frac{B_0^2\sigma_f}{(\rho c_p)_f}$$

$$\chi = \frac{Q_0}{(\rho c_p)_f a}\chi_1 = \frac{k_f}{(\rho c_p)_f v} \tag{18}$$

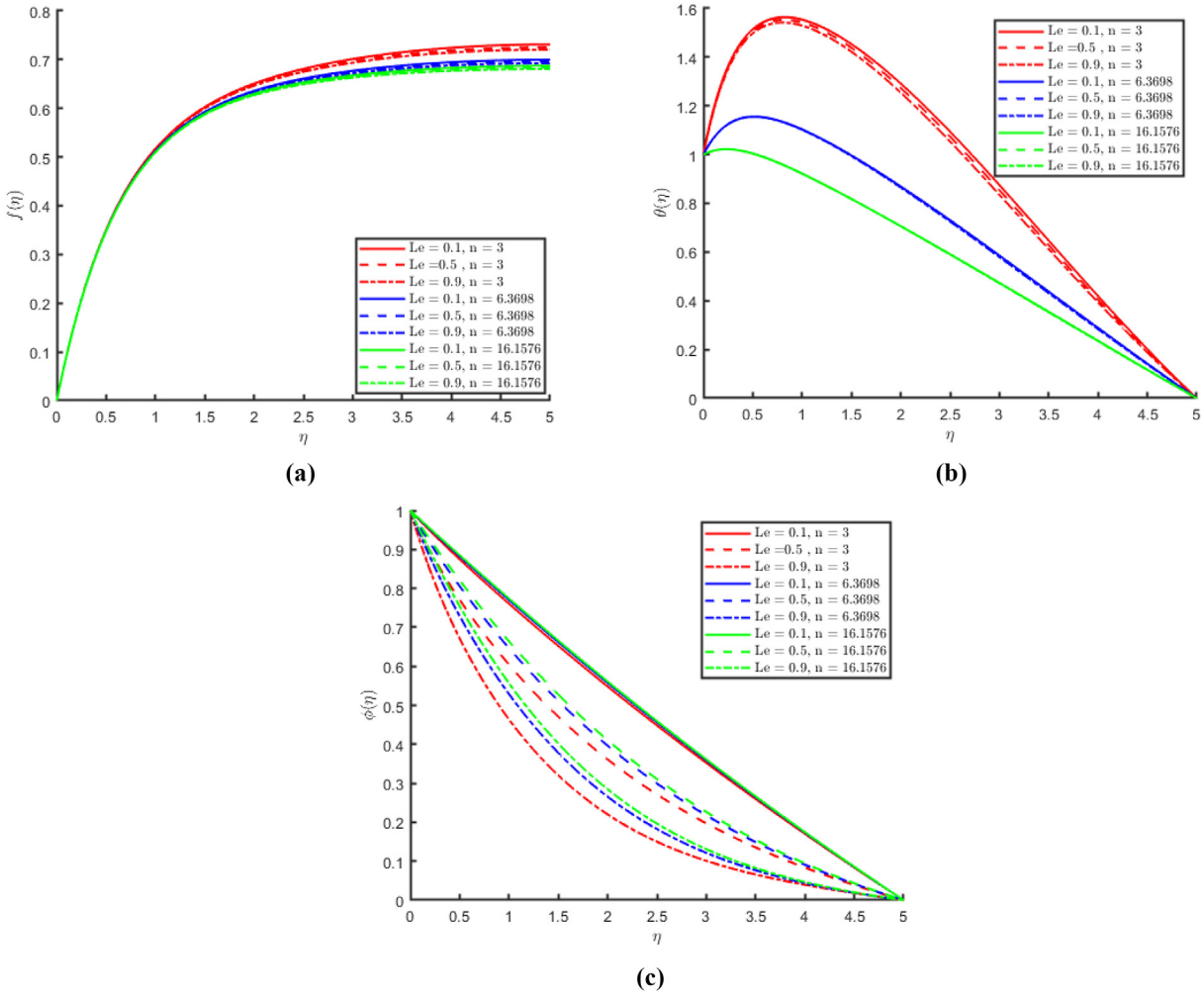

Fig. 5 (a) Representation of the effect of Lewis number on the stream function $f(\eta)$ with different nanoparticle shape sizes. (b) Representation of the effect of Lewis number on the temperature $\theta(\eta)$ with different nanoparticle shape sizes . (c) Representation of the effect of Lewis number on the mass concentration $\phi(\eta)$ with different nanoparticle shape sizes.

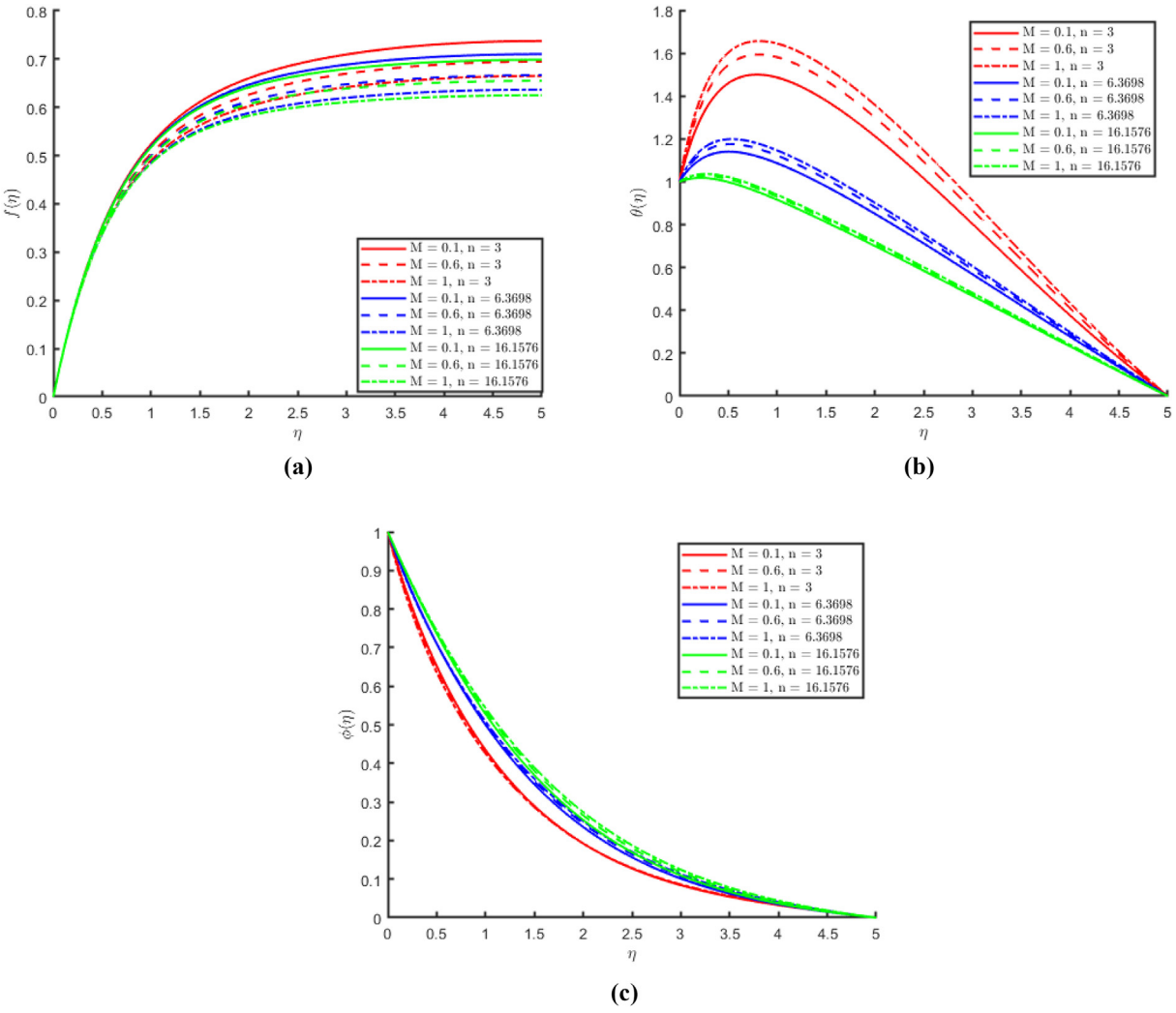

Fig. 6 (a) Representation of the effect of magnetic parameter on the stream function $f(\eta)$ with different nanoparticle shape sizes. (b) Representation of the effect of magnetic parameter on the temperature $\theta(\eta)$ with different nanoparticle shape sizes. (c) Representation of the effect of magnetic parameter on the mass concentration $\phi(\eta)$ with different nanoparticle shape sizes.

where M represents magnetic, Rd radioactivity parameter, Sr Soret number and D_f Dufour effects, N_t is thermophoretic, N_b is Brownian motion, Prandtl number is Pr and L_e is Lewis number.

3. Engineering Quantities of Interest

The skin friction coefficient and Sherwood number are well-defined for this modelled flow issue. The ratio of pure conduction heat transmission to convection heat transfer is known as the Nusselt number. skin friction coefficient is the resistance to the laminar flow of an object moving through a fluid. The proportion of convective mass transfer to mass diffusivity is known as the Sherwood number.

$$C_f = \frac{\tau_z}{\rho_f}, Sh = \frac{xq_m}{k_f(T_w - T_\infty)}, Nu = \frac{q_w}{k_f(T_w - T_\infty)} \tag{19}$$

Where τ_z denotes surface shear stress, q_w represents surface heat flux and q_m defines surface mass flux

$$\tau_z = \mu_{nf}(u_y)_{y=0}, q_m = -D_b(C_y)_{y=0}, q_w = -k\left[\frac{\partial T}{\partial y}\right]_{y=0} \tag{20}$$

Using Eq. (11) in Eq. (17), we have

$$Re_x^{\frac{-1}{2}} C_f = f''(0), \frac{Sh}{\sqrt{Re_x}} = -\phi'(0), Nu(Re_x)_x^{\frac{-1}{2}} = -\theta'(0) \tag{21}$$

0272345433020060-1317745600**Shapes of Nanoparticle**

Thermophysical characteristics of fluid and nanoparticles are given in Table.1. Furthermore, the shapes of nanoparticles are given. In Eqs. 7 and 8 when $n = 3$ the shape of the nanoparticles is spherical and when $n = 6$ then cylindrical. Whereas nanoparticles are laminar when $n = 16$. Shapes of nanoparticles in the presence of a heat source play a dominant role in temperature.

4. Discussions of Graphical and Numerical Results:

In this section, the influence of various physical parameters such as the Dufour effects, Soret effects, Thermophoresis,

Prandtl, Lewis, Maxwell number, Brownian motile, and magnetic field on the stream function, velocity, temperature and concentration profiles have been illustrated with the graphical representations as shown in Figs. 2-11. The numerical solution of linear coupled differential equations is obtained by using the MATLAB software BVP4c method. The spherical-shaped effect (n = 3) $Cu - Al_2O_3$ mixed in ethylene glycol base fluid shows better effects on velocity distributions and temperature profile as compared to the cylindrical and laminar-shaped effect (n = 6.3698, n = 16.1576). However, this behavior reversed in the case of mass concentration. In Fig 2, we analyze the impact of Dufour number and nanoparticle shape on stream function, velocity, temperature, and mass concentration profile with parameter values $\dot{N}_t = 0.1, \beta = 3, \dot{M} = 3, Sr = 0.2, Le = 1, \Pr = 1, \dot{N}_b = 0.8$. It has been observed that with the enhancement in Dufour num-

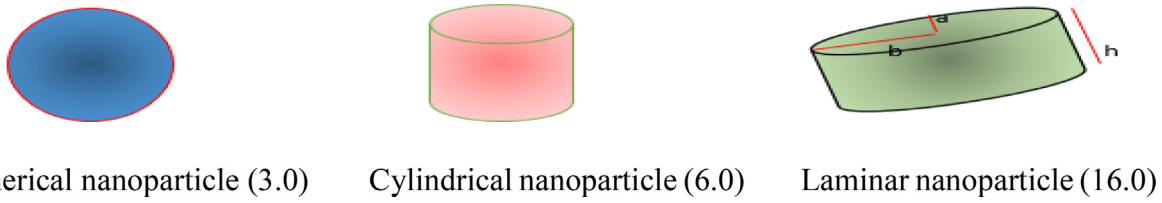

Spherical nanoparticle (3.0) Cylindrical nanoparticle (6.0) Laminar nanoparticle (16.0)

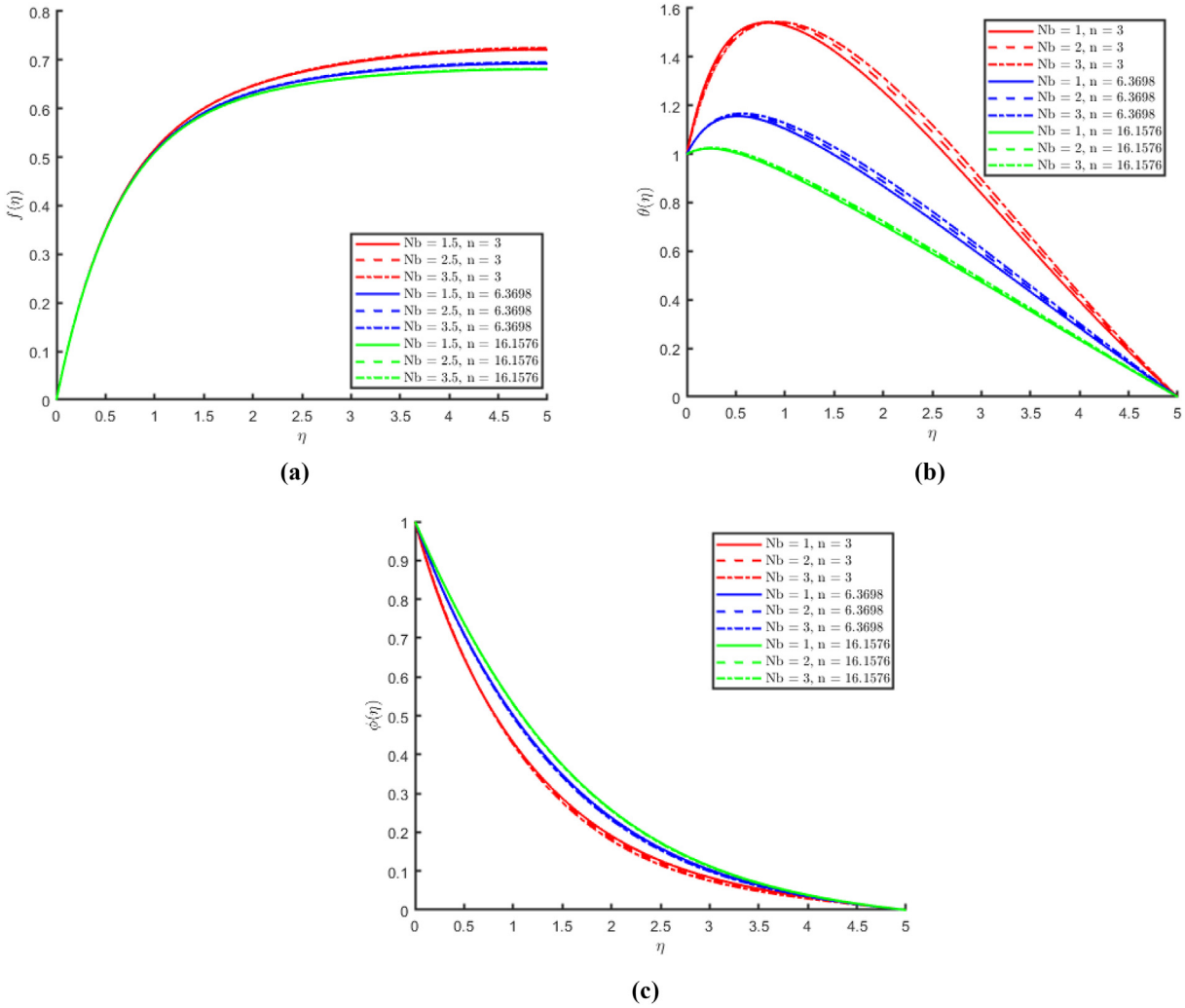

Fig. 7 (a) Representation of the effect of Brownian motion parameter on the stream function $f(\eta)$ with different nanoparticle shape sizes. (b) Representation of the effect of Brownian motion parameter on the temperature $\theta(\eta)$ with different nanoparticle shape sizes. (c) Representation of the effect of Brownian motion parameter on the mass concentration $\phi(\eta)$ with different nanoparticle shape sizes.

ber the stream function $f(\eta)$ and temperature distribution θ decrease for the spherical, cylindrical, and laminar-shaped hybrid nanoparticles. The mass concentration increases with the increase in the Dufour number. The effect of the Dufour number on the stream function $f(\eta)$ and temperature distribution $\theta(\eta)$ is higher in the presence of spherical-shaped nanoparticles as compared to other particle shapes. However, this behavior is the opposite of the mass concentration profile. Fig. 3 represents the impact of Soret number and nanoparticles shape effects on stream function, and the velocity distribution $f'(\eta)$ with $\dot{N}_t = 0.8, \beta = 3, M = 3, Le = 1, \ddot{N}_b = 0.8, D_f = 0.1, \mathrm{P}\dot{r} = 1$. It is observed that with the enhancement in Soret number, the stream function $f(\eta)$, and the velocity distribution increase for spherical, laminar, and cylindrical. This is due to stronger convective flow when Soret number Sr values increase, which causes the boundary layer thickness to grow. Fig 4 illustrates the impact of the Maxwell Parameter and nanoparticle shape effect on stream function and mass concentration with $\mathrm{P}\dot{r} = 1$, $N_b = 0.8$, $M = 3$, $Sr = 0.2$, $D_f = 0.1$, $N_t = 0.1$, $Le = 1$. It is noticed that the stream function decreases when increasing the value of the Maxwell fluid parameter β whereas it is the opposite for mass concentration $\phi(\eta)$ and the temperature distribution $\theta(\eta)$. Physically, the current figures exhibit that the fluid gets more viscous with the increasing values of β which results in the reduction of velocities of the fluid. Moreover, it is also worth mentioning here that the case for viscous HNF can be achieved for $\beta \to \infty$, i.e., the problem will reduce to a Newtonian case. Fig. 5 demonstrates the impact of the Lewis number and nanoparticle shape effect on stream function $f(\eta)$, temperature $\theta(\eta)$, and mass concentration $\phi(\eta)$ with $\mathrm{Pr} = 1, N_b = 0.8, M = 3, \beta = 3, Sr = 0.2, D_f = 0.1, N_t = 0.1$. It has been noticed that the Lewis number has reverse relation with stream function, temperature, and mass concentration.

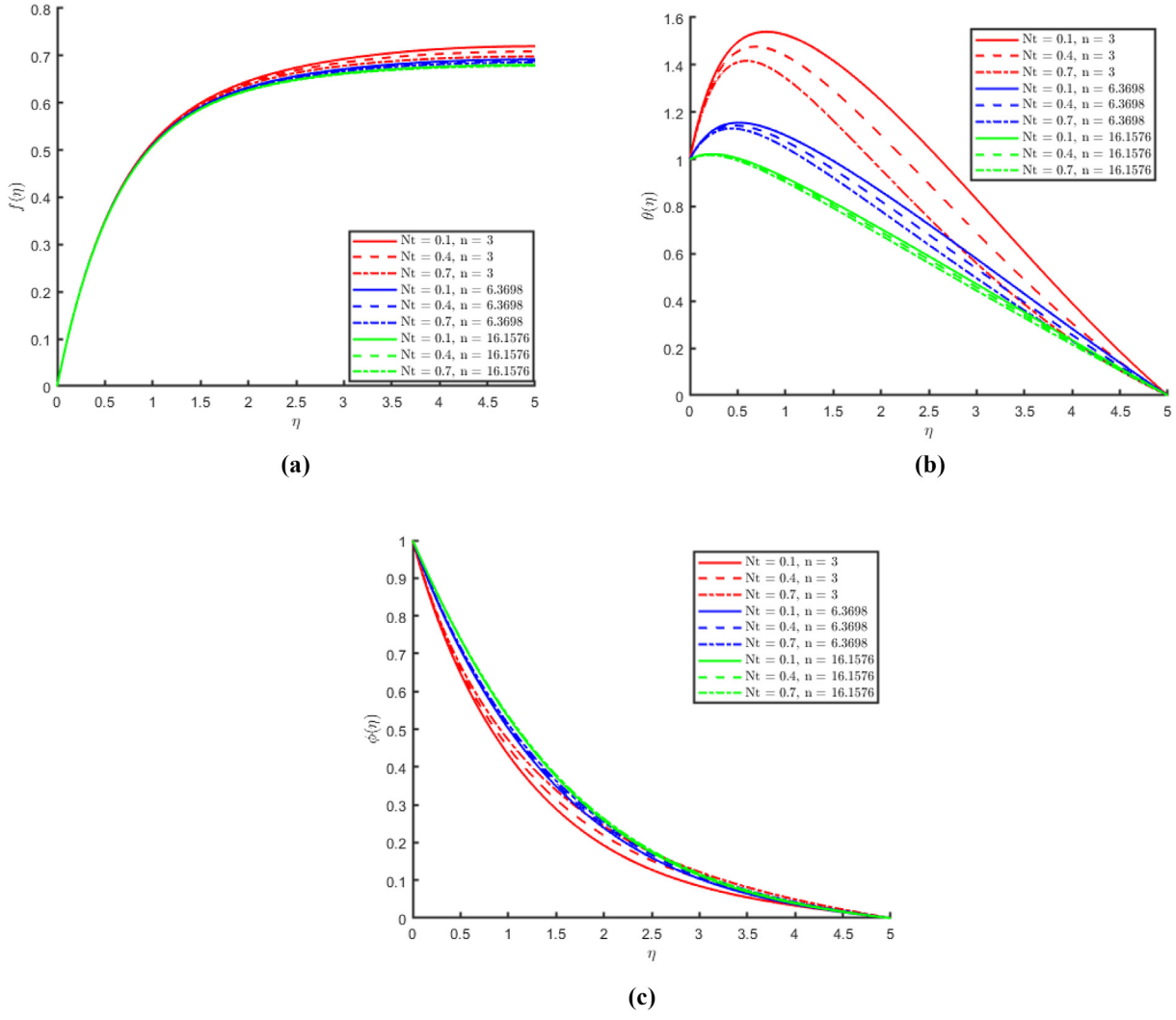

Fig. 8 (a) Representation of the effect of thermophoretic parameters on the stream function $f(\eta)$ with different nanoparticle shape sizes. (b) Representation of the effect of thermophoretic parameters on the temperature $\theta(\eta)$ with different nanoparticle shape sizes. (c) Representation of the effect of thermophoretic parameters on the mass concentration $\phi(\eta)$ with different nanoparticle shape sizes.

Fig 6 exhibits the impact of magnetic field parameter on stream function, mass concentration and temperature profile. In the existence of the magnetic field, it is noticed that the spherical, cylindrical, and laminar-shaped nanoparticles demonstrate an effective role in the stream function and mass concentration distribution with $\mathrm{Pr} = 1, \dot{N}_t = 0.1, S\dot{r} = 0.2, \dot{D}_f = 0.1, Le = 1, \beta = 1, \dot{N}_b = 0.8$. As the imposition of the applied magnetic field produces more resistance to the flow phenomenon, which in turn declines the velocity field. Therefore, due to enhancement in the M the stream function f decreases but the opposite for mass concentration distribution and temperature profile. Magnetic field parameter impact on stream function is better in the case of spherical nanoparticles as compared with Laminar and cylindrical nanoparticles. However, this behavior is the opposite of mass concentration and temperature profile. Fig 7 represents the effect of Brownian motion parameter on stream function, temperature, and mass concentration distribution with $N_t = 0.1, \beta = 3, M = 3, L\dot{e} = 1, \dot{D}_f = 0.1, S\dot{r} = 0.2, \mathrm{Pr} = 1$. Fig 7. (a)-(c) demonstrate that for spherical, cylindrical, and laminar-shaped nanoparticles, the temperature profile $\theta(\eta)$ and stream function profile $f(\eta)$ increase with an increase in the Brownian motion parameter. For all three particles, the Brownian motion parameter declines along with the distribution of mass $\phi(\eta)$. The influence of spherical-shaped nanoparticles on stream function and temperature distribution is higher as compared with mass concentration. When there is a mass concentration, this tendency is reversed. Fig 8 exhibits the impact of thermophoretic parameter on the stream function $f(\eta)$, temperature $\theta(\eta)$ and mass concentration distribution. In Fig. 8(a) it is observed that with the increase in the thermophoretic parameter the stream function $f(\eta)$ decreases with the parameter $\mathrm{Pr} = 1, N_b = 0.8, \beta = 3, M = 3, \dot{D}_f = 0.1, S\ddot{r} = 0.2, L\dot{e} = 1$. Fig 8 (b)-(c) shows that the temper-

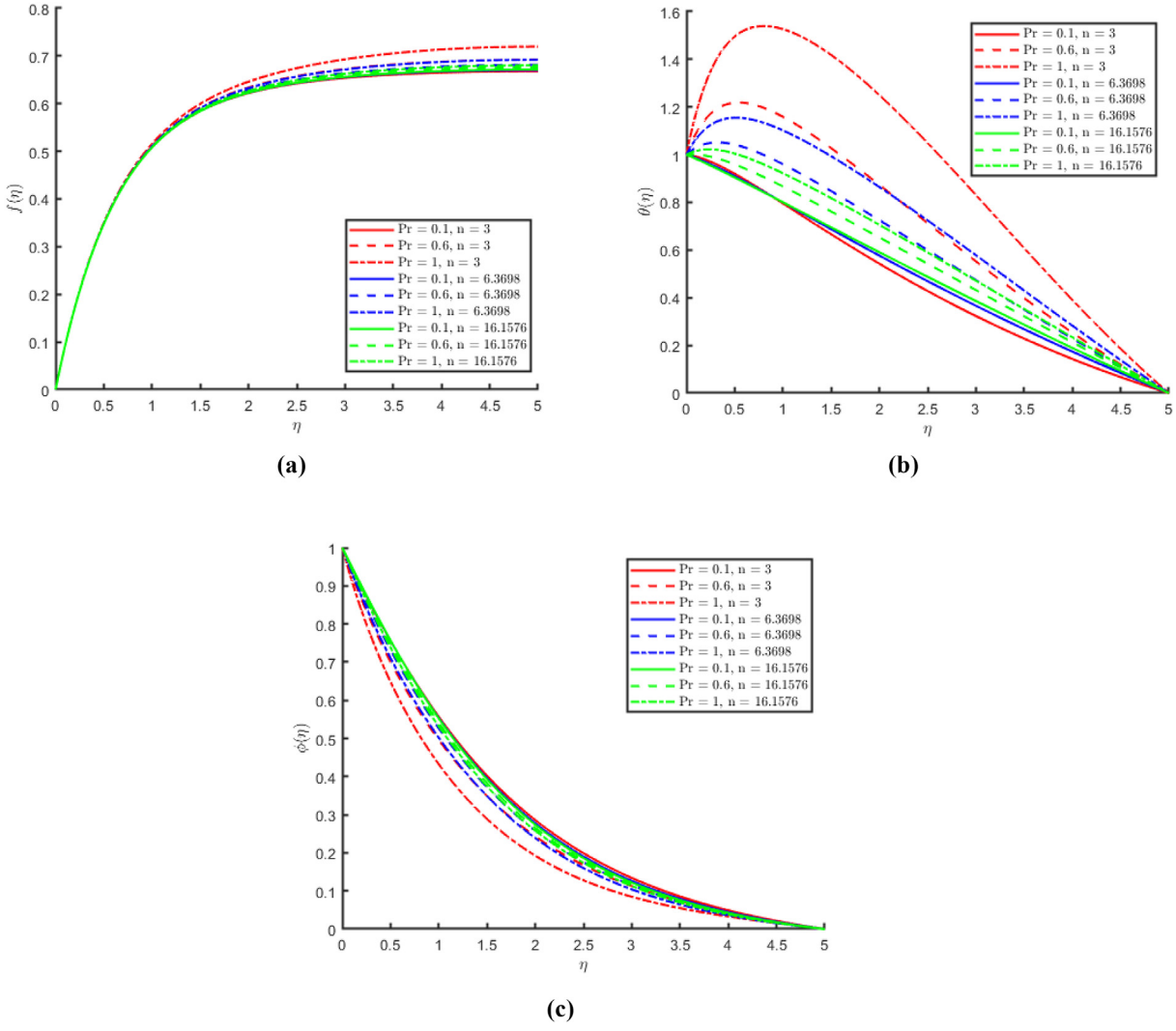

Fig. 9 (a) Representation of the effect of Prandtl number on the stream function $f(\eta)$ with different nanoparticle shape sizes. (b) Representation of the effect of Prandtl number on the temperature $\theta(\eta)$ with different nanoparticle shape sizes. (c) Representation of the effect of Prandtl number on the mass concentration $\phi(\eta)$ with different nanoparticle shape sizes.

ature distribution $\theta(\eta)$ decline with the increase in thermophoretic parameter but exhibits the reverse nature for mass concentration distribution $\phi(\eta)$ with parameters $\mathrm{Pr} = 1, N_b = 0.8, \beta = 3, M = 3, D_f = 0.1, Sr = 0.2, Le = 1$. The influence of spherical-shaped nanoparticles with the variation of thermophoretic parameter on stream function and temperature distribution is higher as compared with mass concentration. This behavior is reversed in the case of mass concentration. Fig. 9 manifests the outcome of Prandtl number on stream function $f(\eta)$, velocity $f'(\eta)$, temperature $\theta(\eta)$ and mass concentration $\phi(\eta)$. In Fig. 9 (a) it is seen that stream function $f(\eta)$ grows when we increase the value of Prandtl number with the parameters $D_f = 0.1$, $\dot{N}_t = 0.1, Sr = 0.2, L\dot{e} = 1, \beta = 1, \ddot{N}_b = 0.8, M = 3$. Fig 9. (b)-(c) represent that the temperature distribution $\theta(\eta)$ increases with the increase in Prandtl number whereas mass concentration $\phi(\eta)$ decreases with the increase in Prandtl number in the presence of parameters $N_b = 0.8, \beta = 3, M = 3, D_f = 0.1$, $Sr = 0.2, Le = 1$. Prandtl number impact on stream function, velocity, the temperature is better than in case of spherical nanoparticles as compared with Laminar and cylindrical nanoparticles. However, this behavior is the opposite of mass concentration. The effect of nanoparticle volume fraction Φ_1 on stream function $f(\eta)$, temperature $\theta(\eta)$, and mass concentration $\phi(\eta)$ is depicted in Fig. 10. Fig. 10 (a)-(c) show that the stream function $f(\eta)$ and the mass concentration decrease as increase the value of nanoparticle Φ_1 while temperature $\theta(\eta)$ increases with the parameters $\mathrm{Pr} = 1, N_b = 0.8, \beta = 3, M = 3, D_f = 0.1, Sr = 0.2, Le = 1$. Fig. 11 represents the impact of nanoparticle Φ_2 on stream function $f(\eta)$, velocity $f'(\eta)$, temperature $\theta(\eta)$ and mass concentration. Fig. 11 (a)-(d) show that the mass concentration

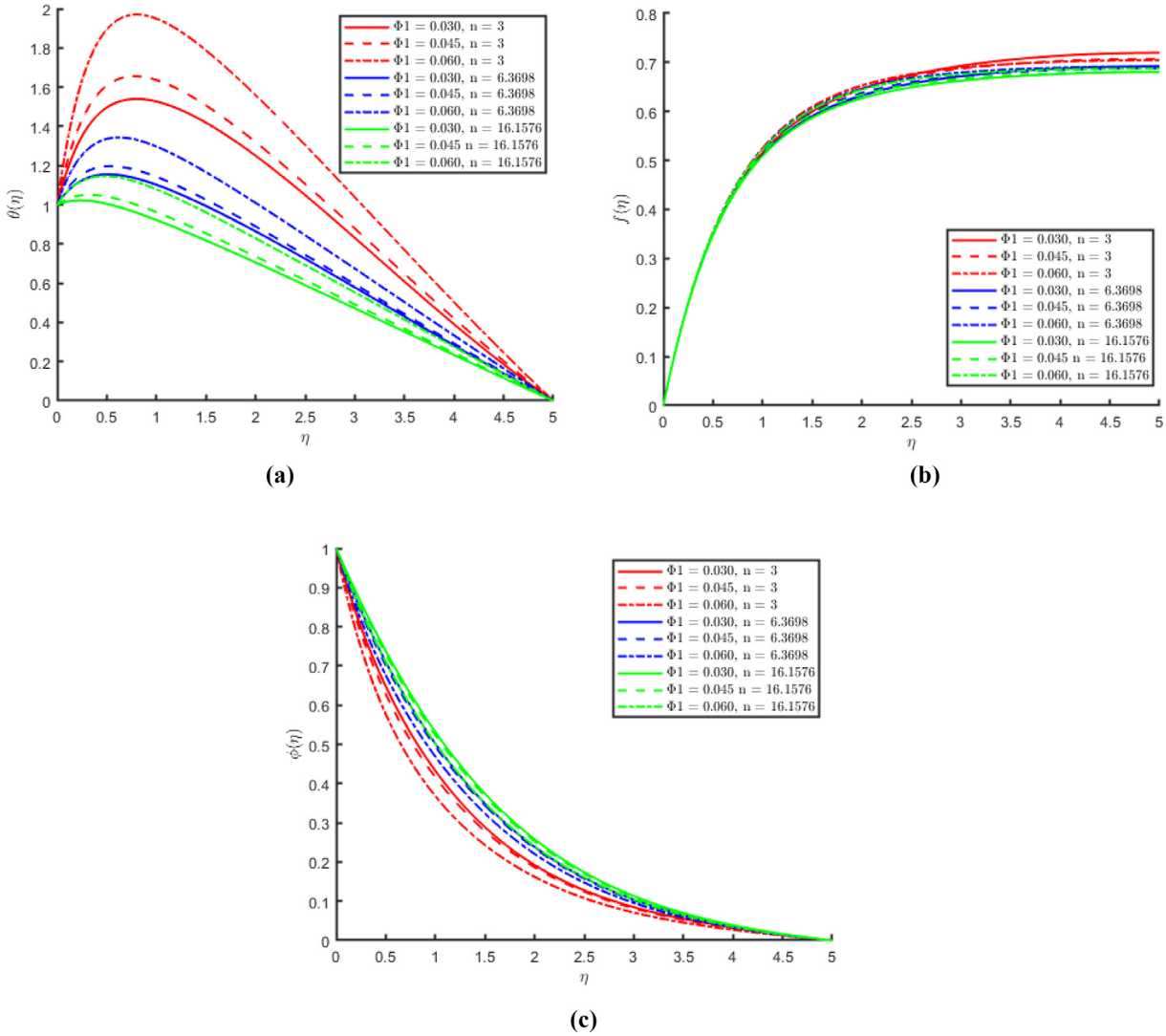

Fig. 10 (a) Representation of the effect of nanoparticle volume fraction Φ_1 on the temperature $\theta(\eta)$ with different nanoparticle shape sizes. (b) Representation of the effect of nanoparticle volume fraction Φ_1 on the steam function $f(\eta)$ with different nanoparticle shape sizes. (c) Representation of the effect of nanoparticle volume fraction Φ_1 on the mass concentration $\phi(\eta)$ with different nanoparticle shape sizes.

$\phi(\eta)$ increases when increasing the value of the nanoparticle Φ_2 but it is the opposite for stream function $f(\eta)$, velocity $f'(\eta)$, and temperature $\theta(\eta)$ with parameters $\Pr = 1, N_b = 0.8, \beta = 3, M = 3, D_f = 0.1, Sr = 0.2, Le = 1$. Figs. 10-11 demonstrate that nanoparticle volume fraction impacts stream function, temperature is better in the case of Laminar nanoparticles as compared with spherical and cylindrical nanoparticles. However, this behavior is the opposite on mass concentration. Both the volume fraction of Alumina/Aluminium oxide and Cuprum/Copper are enhancing the thermal phenomenon. However, the thermal profiles are more prominent in the case of Φ_2 as compared with Φ_1 . The behavior of these figures is agreed with the physical behavior of the nanofluid due to the nanoparticle volume fractions. The thermal conductivity of the nanoparticles is higher than that of base fluid which in turn overall enhances the thermal conductivity of the nanofluid and become the cause of increasing temperature within the boundary layer.

Tables 2-7 represent skin friction coefficient and Sherwood number for distinct values of magnetic M, Prandtl number Pr, Soret effect Sr, Lewis numbers Le and Dufour effect D_f. In Table 2, it is observed that the increment in M increase the SFC and Sherwood number and also decreases the Nusselt number. Table 3 also shows that by increasing the value of the Prandtl number the SFC and Nusselt number decrease and the Sherwood number rises. It is observed that the increment in Sr increase skin friction coefficient and the Nusselt umber and Sherwood number decrease by increment in Sr are shown in Table 4. Table 5 demonstrates the influence of the Le on SFC, Sherwood number and Nusselt number. It is observed that by increment in Le increase the Nusselt number, Sherwood number and decrease SCF. In Table 6. It is observed

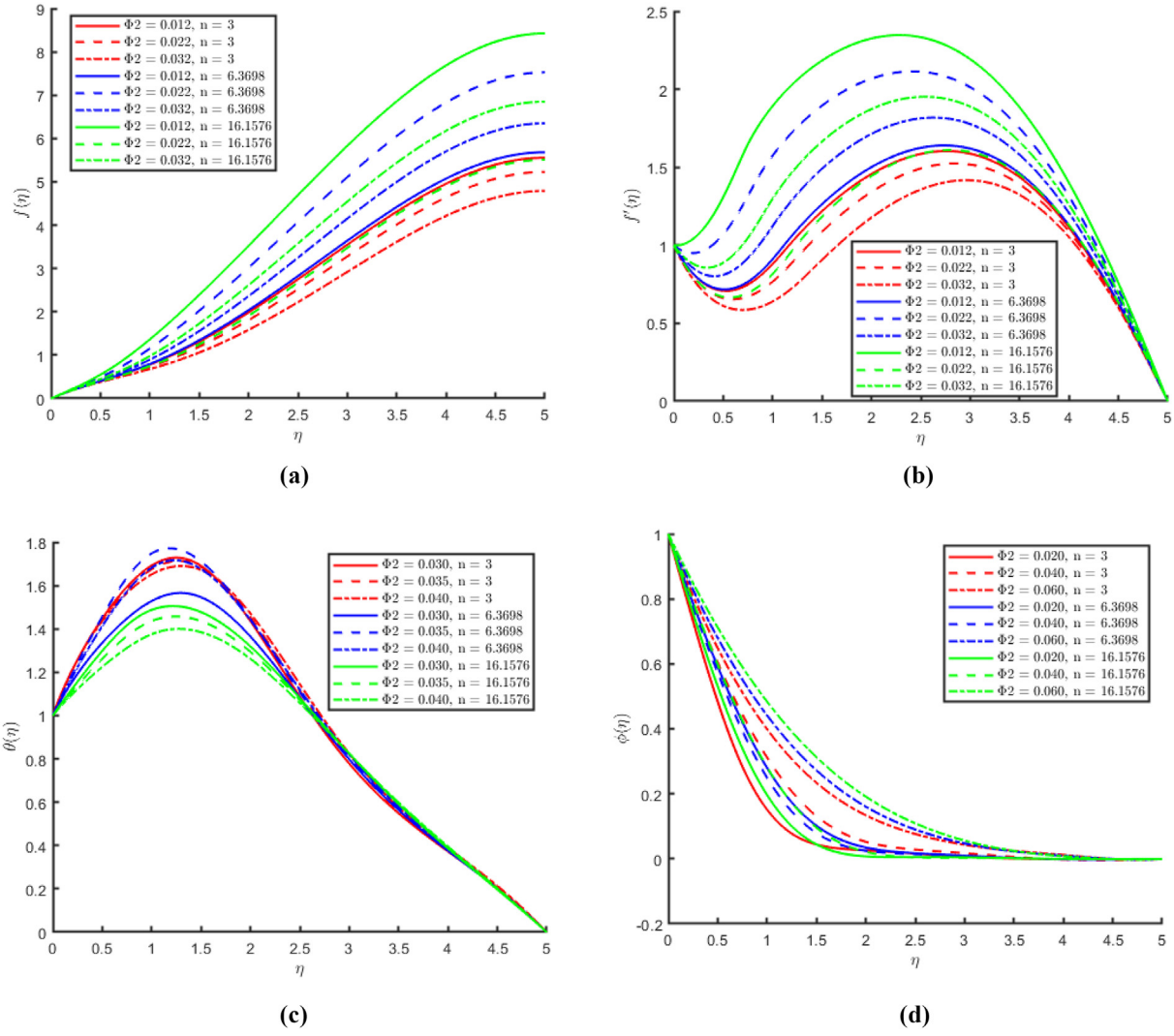

Fig. 11 (a) Representation of the effect of nanoparticle volume fraction Φ_2 on the stream function $f(\eta)$ with different nanoparticle shape sizes. (b) Representation of the effect of nanoparticle volume fraction Φ_2 on the velocity $f'(\eta)$ with different nanoparticle shape sizes. (c) Representation of the effect of nanoparticle volume fraction Φ_2 on the temperature $\theta(\eta)$ with different nanoparticle shape sizes. (d) Representation of the effect of nanoparticle volume fraction Φ_2 on the mass concentration $\phi(\eta)$ with different nanoparticle shape sizes.

Table 2 Represent skin friction coefficient, Sherwood number and Nusslet number for distinct values of magnetic M with $\dot{N}_b = 0.8, \dot{N}_t = 0.1, Df = 0.1, Le = 1, \Pr = 1, \beta = 1, Sr = 0.2$

n	M	$\sqrt{Re_x}Cf$	$Sh(Re_x)^{-\frac{1}{2}}$	$Nu(Re_x)^{-\frac{1}{2}}$
333666161616	0.10.6010.10.6010.10.601	-21.459232-21.323410-21.190571-21.459696-21.399357-21.346732-21.460414-21.435307-21.414503	0.5273110.7473030.9355250.5138600.6137810.6963480.5071680.5492100.583309	2.671201-59.192038-111.6736957.141389-20.819055-43.8169259.362078-2.378953-11.882341

Table 3 Represent skin friction coefficient, Sherwood number and Nusselt number for distinct values of Prandtl number Pr with $\dot{N}_b = 0.8, \dot{N}_t = 0.1, Df = 0.1, Le = 1, M = 3, \beta = 1, Sr = 0.2$

n	Pr	$\sqrt{Re_x}Cf$	$Sh(Re_x)^{-\frac{1}{2}}$	$Nu(Re_x)^{-\frac{1}{2}}$
333666161616	0.10.6010.10.6010.10.601	-20.604719-22.042966-23.134794-20.756651-22.203877-23.299788-20.822891-22.273318-23.370590	0.9087770.9738471.0219960.6877670.7087210.7244200.5831210.5837010.584415	-102.704906-124.447657-140.375088-39.852157-49.466149-56.516903-10.236043-14.228385-17.157504

Table 4 Represent skin friction coefficient, Sherwood number and Nusselt number for distinct values of Soret effect Sr with $\dot{N}_b = 0.8, \dot{N}_t = 0.1, Df = 0.1, Le = 1, M = 3, \Pr = 1, \beta = 1, N_b = 0.8.$

n	Sr	$\sqrt{Re_x}Cf$	$Sh(Re_x)^{-\frac{1}{2}}$	$Nu(Re_x)^{-\frac{1}{2}}$
333666161616	0.511.50.511.50.511.5	-25.377711-23.738930-22.924470-21.355995-21.371217-21.386175-21.418130-21.424155-21.430156	-20.135031-36.836038-55.6962380.9800541.4475691.9086190.7027140.9015101.100043	2027.258991956.910132010.77908-43.593679-43.228130-42.870497-11.874623-11.861714-11.848751

Table 5 Represent skin friction coefficient, Sherwood and Nusselt number for distinct values of Lewis numbers Le with $\dot{N}_b = 0.8, \dot{N}_t = 0.1, Df = 0.1, M = 3, \Pr = 1, \beta = 1, Sr = 0.2,$

N	Le	$\sqrt{Re_x}Cf$	$Sh(Re_x)^{-\frac{1}{2}}$	$Nu(Re_x)^{-\frac{1}{2}}$
333666161616	0.10.50.90.10.50.90.10.50.9	-21.143559-21.165572-21.185929-21.317307-21.330789-21.343718-21.389164-21.400706-21.411885	0.2733420.5720160.8647620.2466360.4439820.6464430.2346830.3852820.543861	-116.098194-114.099876-112.137738-44.116233-44.012358-43.859540-11.811231-11.853569-11.878580

Table 6 Represent skin friction coefficient, Sherwood and Nusselt number for distinct values of Dufour effect D_f with $\dot{N}_b = 0.8, \dot{N}_t = 0.1, Le = 1, M = 3, \Pr = 1, \beta = 1, Sr = 0.2,$

N	D_f	$\sqrt{Re_x}Cf$	$Sh(Re_x)^{-\frac{1}{2}}$	$Nu(Re_x)^{-\frac{1}{2}}$
333666161616	1.52.53.51.52.53.51.52.53.5	-21.284223-21.319436-21.342987-21.367785-21.378634-21.387226-21.418434-21.420860-21.423025	0.7955710.7402650.7024280.6618460.6438510.6294950.5765770.5724130.568691	-71.904610-56.240547-45.536311-34.064113-28.979468-24.924283-9.981678-8.806366-7.755614

Table 7 Comparison of the flow of nanofluid and hybrid nanofluid for various values of Prandtl number Pr with $\alpha = 0.1, \beta = 1, \gamma = 2, D_f = 0.1, N_b = 0.8, N_t = 0.1, Sr = 0.2, M = 03, Le = 1$.

Parameter	Skin friction C_f		Sherwood Number Sh	
Pr	Al_2o_3-EGnanoparticle	Al_2o_3-C_u/EGHybrid nanoparticle	Al_2o_3-EGnanoparticle	Al_2o_3-C_u/EGHybrid nanoparticle
0.1	-1.8695	-1.6096	0.2770	0.2859
0.2	-2.2865	-2.0772	0.3612	0.3710
0.3	-2.5505	-2.3687	0.4156	0.4250
0.4	-2.7429	-2.5790	0.4546	0.4635

that by increasing the Nusselt number and Sherwood number, SCF decreases when increasing the value of D_f.

Tables 8-12 display a comparison of numerical values of skin friction coefficient and Sherwood number against the above-mentioned parameters with that of (Al_2o_3-EG) nanofluid and (Al_2o_3-C_u/EG) hybrid nanofluid, and in these tables ($\Phi_1 = 0.1$ and $\Phi_2 = 0.1$) in the case of hybrid nanofluid, and ($\Phi_1 = 0$ and $\Phi_2 = 0.2$)in the case of nanofluid.

It has been shown that the hybrid nanofluid has superior shear stress/skin friction and Sherwood number/surface mass flux than nanofluid flow. It is observed that the increment in M decrease the SFC and Sherwood numbers for both cases. It is also observed that the increment in Pr decrease the SFC and increases the Sherwood number for both cases. Moreover, when increasing the value of Sr the SCF and Sherwood number increases for both cases.

Table. 13 compares the limiting situation and shows that when alternative ideologies of the Prandtl number and suction/injection parameter are taken into account, there is extremely excellent agreement for the Nusselt number.

Table 8 Comparison of the flow of nanofluid and hybrid nanofluid for various values of Dufour number D_f with $\alpha = 0.1$, $\beta = 1$, $\gamma = 2$, Pr = 1, $N_b = 0.8$, $N_t = 0.1$, Sr = 0.2,M = 0.3,Le = 1.

Parameter	Skin friction C_f		Sherwood Number Sh	
D_f	Al_2o_3-EGnanoparticle	Al_2o_3-C_u/EGHybrid nanoparticle	Al_2o_3-EGnanoparticle	Al_2o_3-C_u/EGHybrid nanoparticle
0.1	-3.3887	-3.2744	0.5614	0.5680
0.3	-3.4605	-3.3528	0.5515	0.5575
0.5	-3.5371	-3.4363	0.5401	0.5455
0.7	-3.6195	-3.5262	0.5270	0.5315

Table 9 Comparison of the flow of nanofluid and hybrid nanofluid for various values of magnetic field parameter M with $\alpha = 0.1$, $\beta = 1$, $\gamma = 2$, Pr = 1, $N_b = 0.8$, $N_t = 0.1$, Sr = 0.2, $D_f = 0.1$, Le = 1.

Parameter	Skin friction C_f		Sherwood Number Sh	
M	Al_2o_3-EGNanoparticle	Al_2o_3-C_u/EGHybrid nanoparticle	Al_2o_3-EG nanoparticle	Al_2o_3-C_u/EG Hybrid nanoparticle
0.1	-2.0934	-1.9934	0.6395	0.6443
0.4	-2.2509	-2.1484	0.6291	0.6343
0.7	-2.4014	-2.2968	0.6194	0.6249
01	-2.5457	-2.4393	0.6103	0.6161

Table 10 Comparison of the flow of nanofluid and hybrid nanofluid for various values of Lewis number Le with $\alpha = 0.1$, $\beta = 1$, $\gamma = 2$, Pr = 1, M = 0.3, $N_t = 0.1$, Sr = 0.2, $D_f = 0.1$, $N_b = 0.1$.

Parameter	Skin friction C_f		Sherwood Number Sh	
Le	Al_2o_3-EGnanoparticle	Al_2o_3-C_u/EGHybrid nanoparticle	Al_2o_3-EGnanoparticle	Al_2o_3-C_u/EGHybrid nanoparticle
0.2	-3.5259	-3.2744	0.2774	0.5680
0.5	-3.4682	-3.2180	0.3847	0.6467
0.8	-3.4167	-3.1417	0.4932	0.7171
1.1	-3.3765	-3.0340	0.5940	0.7778

Table 11 Comparison of the flow of nanofluid and hybrid nanofluid for various Soret number Sr values with $\alpha = 0.1$, $\beta = 1$, $\gamma = 2$, Pr = 1, M = 0.3, Le = 1, $N_t = 0.1$, $D_f = 0.1$, $N_b = 0.1$.

Parameter	Skin friction C_f		Sherwood Number Sh	
Sr	Al_2o_3-EGnanoparticle	Al_2o_3-C_u/EGHybrid nanoparticle	Al_2o_3-EGnanoparticle	Al_2o_3-C_u/EGHybrid nanoparticle
0.3	-3.3737	-3.2574	0.5885	0.5951
0.6	-3.3189	-3.1953	0.6647	0.6711
0.9	-3.2434	-3.1101	0.7322	0.7385
1.2	-3.1342	-2.9879	0.7891	0.7955

Table 12 Comparison of $\theta'(0)$ for some values of Pr and Sr when $\beta = \gamma = \lambda = D_f = N_t = \phi = N_b = 0$

S	Pr	Ishak et al. (Hayat et al., 2011)	Hayat et al. [53]	Present
-1.5	0.72	0.4570	0.4570273	0.4570271
	1	0.5000	0.5000000	0.5000000
	10	0.6542	0.6451648	0.6451643
0	0.72	0.8086	0.8086314	0.8086312
	1	1.0000	1.0000000	1.0000000
	3	1.9237	1.92359132	1.9359131
	10	3.7207	3.7215968	3.7215955
1.5	0.72	1.4944	1.4943687	1.4943684
	1	2.0000	2.0000621	2.0000619
	10	16.0842	16.096248	16.096236

Conclusion: In this paper, Examining the consequences of mixed convection, Soret and Dufour flow via a porous Maxwell hybrid nanofluid medium is of significant interest in this investigation on linearly stretchable sheet. On a stretched, linearly porous surface, the effects of altering temperature and concentration are also taken into account. And the comparison of nanoparticles and hybrid nanoparticles is discussed. Results were compared by graphical and numerical solutions with the help of Bvp4c MATLAB software. The problem and proposed result are both unique and have not before been covered in the literature. The following list includes the study's key conclusions: In the presence of the magnetic field parameter, the stream function increased.

- The existence of the Prandtl number reaction reduces the mass concentration profile and increases in the presence of Brownian motion.
- In the convection flow of different parameters Dufour number, Lewis number and Thermophoretic parameter increase temperature distribution decrease.
- In the existence of Soret and Prandtl number velocity profile increases.
- The nanoparticle shape factor shows a powerful aspect of the temperature profile.
- In general, spherical-shaped nanoparticles have a better impact on stream function, velocity and temperature distributions. This behavior is the opposite of the mass concentration profiles.

Data Availability Statement:

Not applicable

References:

Zierep, J., Fetecau, C., 2007. Energetic balance for the Rayleigh-Stokes problem of a Maxwell fluid. Int. J. Eng. Sci. 45, 617–627.

Fetecau, C., Athar, M., Fetecau, C., 2009. Unsteady flow of Maxwell fluid with fractional derivative due to a constantly accelerating plate. Comput. Math. Appl. 57, 596–603.

Choi, S.U.S., 1995. Enhancing thermal conductivity of fluids with nanoparticles. Proc ASME Int Mech Eng Congr Expo 66, 99–105.

Shehzad, S.A., Abdullah, Z., Alsaedi, A., Abbasi, F.M., Hayat, T., 2016. Thermally radiative three-dimensional flow of Jeffrey nanofluid with internal heat generation and magnetic field. J Magn Magn Mater 397 (1), 108–114.

Hayat T, T, Muhammad, Shehzad SA, Alsaedi A. On three-dimensional boundary layer flow of Sisko nanofluid with magnetic field effects. Adv

Powder Technol 2016;27(2):504–12.Khan JA, Mustafa M, Mushtaq A. On three-dimensional flow of nanofluids past a convectively heated deformable surface: A numerical study. Int J Heat Mass Transfer 2016;94:49–55.

Dogonchi, A.S., Ganji, D.D., 2016. Investigation of MHD nanofluid flow and heat transfer in a stretching/shrinking convergent/divergent channel considering thermal radiation. J Mol Liq 220, 592–603.

Ramzan, M., Bilal, M., 2016. Three-dimensional flow of an elastico-viscous nanofluid with chemical reaction and magnetic field effects. J Mol Liq 215, 212–220.

Kumar, M., Dinesh, C.S.K., Raju, K.S., El-Zahar, E.R., Shah, N.A., 2022. Linear and quadratic convection on 3D flow with transpiration and hybrid nanoparticles. International Communications in Heat and Mass Transfer 134, 105995.

Sajjan, K., Shah, N.A., Ameer Ahammad, N., Raju, C.S.K., Dinesh Kumar, M., Weera, W., 2022. Nonlinear Boussinesq and Rosseland approximations on 3D flow in an interruption of Ternary nanoparticles with various shapes of densities and conductivity properties. AIMS Math 7 (10), 18416–18449.

Abderrahmane, A., Qasem, N.AA., Younis, O., Marzouki, R., Mourad, A., Shah, N.A., Chung, J.D., 2022. MHD hybrid

nanofluid mixed convection heat transfer and entropy generation in a 3-D triangular porous cavity with zigzag wall and rotating cylinder. Mathematics 10 (5), 769.
Rauf, A., Mushtaq, A., Shah, N.A., Botmart, T., 2022. Heat transfer and hybrid ferrofluid flow over a nonlinearly stretchable rotating disk under the influence of an alternating magnetic field. Scientific Reports 12 (1), 17548.
Buongiorno, Jacopo. "Convective transport in nanofluids." (2006): 240-250.
Akbar N, Khan Z, Nadeem S, Khan W. Double-diffusive natural convective boundary-layer flow of a nanofluid over a stretching sheet with magnetic field.
Mustafa, M., Khan, J.A., Hayat, T., Alsaedi, A., 2017. Buoyancy effects on the MHD nanofluid flow past a vertical surface with chemical reaction and activation energy. International Journal of Heat and Mass Transfer 108, 1340–1346.
Hsiao, K.-L., 2017. To promote radiation electrical MHD activation energy thermal extrusion manufacturing system efficiency by using Carreau-Nanofluid with parameters control method. Energy 130, 486–499.
Zeeshan, A., Shehzad, N., Ellahi, R., 2018. Analysis of activation energy in Couette-Poiseuille flow of nanofluid in the presence of chemical reaction and convective boundary conditions. Results in Physics 8, 502–512.
Hassan, M., Marin, M., Alsharif, A., Ellahi, R., 2018. Convective heat transfer flow of nanofluid in a porous medium over wavy surface. Phys Lett 382(38):2749e53.
Ahmad, L., Khan, M., 2019. Importance of activation energy in development of chemical covalent bonding in flow of Sisko magneto-nanofluids over a porous moving curved surface. International Journal of Hydrogen Energy 44 (21), 10197–10206.
Layek, G.C., Mandal, B., Bhattacharyya, K., Banerjee, A., 2018. Lie symmetry analysis of boundary layer stagnation-point flow and heat transfer of non-Newtonian power-law fluids over a nonlinearly shrinking/stretching sheet with thermal radiation. International Journal of Nonlinear Sciences and Numerical Simulation 19 (3–4), 415–426.
Khan, M., Sarfraz, M., Ahmed, J., Ahmad, L., Fetecau, C., 2020. Non-axisymmetric Homann stagnation-point flow of Walter's B nanofluid over a cylindrical disk. Applied Mathematics and Mechanics 41 (5), 725–740.
Ahmad, L., Khan, M., 2019. Numerical simulation for MHD flow of Sisko nanofluid over a moving curved surface: A revised model. Microsystem Technologies 25, 2411–2428.
Mukhopadhyay, S., Layek, G.C., Samad, S.A., 2005. Study of MHD boundary layer flow over a heated stretching sheet with variable viscosity. International journal of heat and mass transfer 48 (21–22), 4460–4466.
Shafique, Z., Mustafa, M., Mushtaq, A., 2016. Boundary layer flow of Maxwell fluid in rotating frame with binary chemical reaction and activation energy. Results Phys 6, 627–633.
Khader, M.M., Megahed, A.M., 2016. Numerical treatment for flow and heat transfer of Powell-Eyring fluid over an exponential stretching sheet with variable thermal conductivity. Meccanica 51 (8), 1763–1767.
Abbas, Z., Sheikh, M., Motsa, S.S., 2016. Numerical solution of binary chemical reaction on stagnation point flow of Casson fluid over a stretching/shrinking sheet with thermal radiation. Energy 95, 12–20.
Ramzan, M., Farooq, M., Alsaedi, A., Hayat, T., 2013. MHD three-dimensional flow of couple stress fluid with Newtonian heating. Eur Phys J Plus 128, 49–64.
Türk, Ö., Sezgin, M.T., 2016. FEM solution to natural convection flow of a micropolar nanofluid in the presence of a magnetic field. Meccanica, 1–13.
Ramzan, M., Farooq, M., Alhothuali, M.S., Malaikah, H.M., Cui, W., Hayat, T., 2015. Three dimensional flow of an Oldroyd-B fluid with Newtonian heating. Int J Numer Methods Heat Fluid Flow 25 (1), 68–85.
Hayat, T., Aziz, A., Muhammad, T., Ahmad, B., 2016. On magnetohydrodynamic flow of second grade nanofluid over a nonlinear stretching sheet. J Magn Magn Mater 408, 99–106.
Hayat, T., Ashraf, M.B., Alsulami, H., Alhuthali, M.S., 2014. Three-dimensional mixed convection flow of viscoelastic fluid with thermal radiation and convective conditions. PLoS One 9 (3), e90038.
Ramzan, M., Farooq, M., Hayat, T., Chung, J.D., 2016. Radiative and Joule heating effects in the MHD flow of a micropolar fluid with partial slip and convective boundary condition. J Mol Liq 221, 394–400.
Mustafa, M., Mushtaq, A., Hayat, T., Alsaedi, A., 2016. Rotating flow of magnetite-water nanofluid over a stretching surface inspired by non-linear thermal radiation. PLoS One 11 (2), e0149304.
Ali, N., Khan, S.U., Abbas, Z., Sajid, M., 2016. Soret and Dufour effects on hydromagnetic flow of viscoelastic fluid over porous oscillatory stretching sheet with thermal radiation. J Braz Soc Mech Sci, 1–14.
Pal, D., Roy, N., Vajravelu, K., 2016. Effects of thermal radiation and Ohmic dissipation on MHD Casson nanofluid flow over a vertical non-linear stretching surface using scaling group transformation. Int J Mech Sci 114, 257–267.
Mabood F, Pochai N. Analytical investigation of magnetohydrodynamic flow over a nonlinear porous stretching sheet. Adv. Math. Phys. 2016 (Article ID 7821405, 6 pages).
3M. Renardy and X. Wang, "Boundary layers for the upper convected Maxwell fluid," J. Non-Newtonian Fluid Mech. **189-190**, 14–18 (2012).
Hayat, T., Awais, M., Qasim, M., Hendi, A.A., 2011. Effects of mass transfer on the stagnation point flow of an upper convected Maxwell fluid. Int. J. Heat Mass Transfer 54 (15–16), 3777–3782.
Hayat, T., Awais, M., Sajid, M., 2011. Mass transfer effects on the unsteady flow of UCM fluid over a stretching sheet. Int. J. Mod. Phys. B 25, 2863–2878.
Abbasbandy, S., Naz, R., Hayat, T., Alsaedi, A., 2014. Numerical and analytical solutions for Falkner-Skan flow of MHD Maxwell fluid. Appl. Math. Comput. 242, 569–575.
Mustafa, M., Khan, J.A., Hayat, T., Alsaedi, A., 2015. Simulations for Maxwell fluid flow past a convectively heated exponentially stretching sheet with nanoparticles. AIP Adv. 5, (3) 037133.
Awais, M., Hayat, T., Irum, S., Alsaedi, A., 2015. Heat generation/absorption effects in a boundary layer stretched flow of Maxwell nanofluid: Analytic and numeric solutions. PLoS One 10 (6), e0129814.
Sidra, A., Khan, I., Ismail, Z., Salleh, M.Z., Qasem, M.-A.-M., 2017. Heat transfer enhancement in free convection flow of CNTs Maxwell nanofluids with four different types of molecular liquids. Sci. Rep. 7 (1), 2445.
Asim, A., Jamshed, W., Aziz, T., 2018. Mathematical model for thermal and entropy analysis of thermal solar collectors by using Maxwell nanofluids with slip conditions, thermal radiation and variable thermal conductivity. Open Phys. 16 (1), 123–136.
Alireza, R., Abbasi, M., Rahimipetroudi, I., Sunden, B., Ganji, D.D., Gholami, M., 2018. Heat transfer and MHD flow of non-Newtonian Maxwell fluid through a parallel plate channel: Analytical and numerical solution. Mech. Sci. 9 (1), 61–70.
Rauf, A., Shah, N.A., Mushtaq, A., Botmart, T., 2023. Heat transport and magnetohydrodynamic hybrid micropolar ferrofluid flow over a non-linearly stretching sheet. AIMS Mathematics 8 (1), 164–193.
Bird, R.B., Armstrong, R.C., Hassager, O., 1987. "Dynamics of polymeric liquids. Vol. 1: Fluid mechanics.".
Maxwell, J.C., "iv., 1867. On the dynamical theory of gases.". Philosophical transactions of the Royal Society of London 157, 49–88.

Deville, M., Gatski, T.B., 2012. Mathematical modeling for complex fluids and flows. Springer Science & Business Media.

Jawad, M., Saeed, A., Khan, A., Ali, I., Alrabaiah, H., Gul, T., Bonyah, E., Zubair, M., 2021. Analytical study of MHD mixed convection flow for Maxwell nanofluid with variable thermal conductivity and Soret and Dufour effects. AIP Advances 11, (3) 035215.

Ishak, A., Nazar, R., Pop, I., 2009. Heat transfer over an unsteady stretching permeable surface with prescribed wall temperature. Nonlinear Analysis: Real World Applications 10 (5), 2909–2913.

Hayat, T., Qasim, M., Mesloub, S., 2011. MHD flow and heat transfer over permeable stretching sheet with slip conditions. International Journal for Numerical Methods in Fluids 66 (8), 963–975.